Front. Chem. Sci. Eng. 2021, 15(6): 1514–1523
https://doi.org/10.1007/s11705-021-2092-4

RESEARCH ARTICLE

Thermoresponsive block copolymer supported Pt nanocatalysts for base-free aerobic oxidation of 5-hydroxymethyl-2-furfural

Huaxin Qu[1*], Jie Deng[1*], Bei Wang[1], Lezi Ouyang[1], Yong Tang[1], Kai Yu[2], Lan-Lan Lou (✉)[1], Shuangxi Liu[1,3]

1 Institute of New Catalytic Materials Science, School of Materials Science and Engineering, National Institute for Advanced Materials, Nankai University, Tianjin 300350, China
2 MOE Key Laboratory of Pollution Processes and Environmental Criteria and Tianjin Key Laboratory of Environmental Technology for Complex Transmedia Pollution, College of Environmental Science and Engineering, Nankai University, Tianjin 300350, China
3 MOE Key Laboratory of Advanced Energy Materials Chemistry, Collaborative Innovation Center of Chemical Science and Engineering (Tianjin), Tianjin 300072, China

Abstract A base-free catalytic system for the aerobic oxidation of 5-hydroxymethyl-2-furfural was exploited by using Pt nanoparticles immobilized onto a thermoresponsive poly(acrylamide-*co*-acrylonitrile)-*b*-poly(*N*-vinylimidazole) block copolymer, with an upper critical solution temperature of about 45 °C. The Pt nanocatalysts were well-dispersed and highly active for the base-free oxidation of 5-hydroxymethyl-2-furfural by molecular oxygen in water, affording high yields of 2,5-furandicarboxylic acid (up to > 99.9%). The imidazole groups in the block copolymer were conducive to the improvement of catalytic performance. Moreover, the catalysts could be easily separated and recovered based on their thermosensitivity by cooling the reaction system below the upper critical solution temperature. Good stability and reusability were observed over these copolymer-immobilized catalysts with no obvious decrease in catalytic activity in the five consecutive cycles.

Keywords aerobic oxidation, base-free, 5-hydroxymethyl-2-furfural, Pt nanoparticle, thermoresponsive block copolymer

1 Introduction

Biomass has been considered to be the most attractive sustainable sources for fuels and bulk chemical feedstocks [1–5]. 5-Hydroxymethyl-2-furfural (HMF), one of the major biomass platform chemicals, can be obtained from acid-catalyzed dehydration of cellulose and its derived C6 carbohydrates can be converted into a variety of biofuels, fine chemicals and pharmaceuticals [6–8]. Recently, the oxidation of HMF has attracted increasing attention since its final product, 2,5-furandicarboxylic acid (FDCA), has been listed as one of the top 12 building-block chemicals by the US Department of Energy and is regarded as a promising alternative to petroleum-derived terephthalic acid for the manufacture of key polyesters and polyamides [9–12]. A wide variety of metal catalysts, especially noble metal nanocatalysts, such as Au [13,14], Pt [15–17], Pd [18–20], Ru [21] and Au-Pd alloy [22,23], supported on different carriers, including metal oxides [13,16–18], carbon materials [21,22], zeolite [14], hydroxyapatite [20] and zinc hydroxycarbonate [23], have been developed for the catalytic aerobic oxidation of HMF toward FDCA in water with satisfactory catalytic efficiency by using molecular oxygen or air as the green oxidant. In most cases, however, a large excess of homogeneous base, such as NaOH or Na_2CO_3, was required, greatly limiting their practical applications due to the potential equipment corrosion and environmental pollution, as well as the need of neutralization reaction to isolate the acid products.

Consequently, it is highly desirable to develop new catalyst systems for the aerobic oxidation of HMF without the use of homogeneous base. Some progress has been achieved. Hydrotalcite- or basic oxide-supported Au [24–26], Pd [27] and Au-Pd alloy [28,29] nanocatalysts were reported to be active for the aerobic oxidation of HMF toward FDCA in water in the absence of a liquid base. However, the instability of these solid base supports under

Received April 16, 2021; accepted July 16, 2021

E-mail: lllou@nankai.edu.cn

*These authors contributed equally to this work.

the reaction conditions was always an issue, and partial dissolution of the support often occurred. Different carbonaceous materials such as functionalized carbon nanotube [30,31], activated carbon [32], and N-doped carbon materials [33–35] were applied to support Au-Pd alloy, Pt or Ru catalysts for the base-free oxidation of HMF to FDCA in the aqueous phase, but the corresponding Ru catalysts exhibited relatively low catalytic activities with the yields of FDCA no more than 90%. Whereas Mn-Ce [36] or Mn-Co [37] mixed oxide-supported Ru nanocatalysts demonstrated high catalytic performance ($>99\%$ FDCA yields), due mainly to the strong metal-support interaction and unique support composition. Pt supported on other solid base materials, such as C–O–Mg [38] and N-doped carbon decorated CeO_2 [39], were reported to be efficient and stable catalysts for the aqueous-phase aerobic oxidation of HMF to FDCA without a homogeneous base, in which the surface structures and properties of the supports were crucial.

It can be noticed that some attention has been paid to the inorganic solid material-supported nanocatalysts for the liquid-base-free aerobic oxidation of HMF to FDCA, however, the reports about the organic polymer-based catalysts to date have been very limited. Siankevich et al. [40] reported the Pt nanocatalysts stabilized by an ionic polymer (IP) or polyvinyl pyrrolidone (PVP) for the oxidation of HMF in water without the addition of any liquid base. IP was a porous solid that was insoluble in water, and the corresponding catalyst Pt/IP was active and stable for the oxidation reaction. While Pt/PVP that was well-dispersed in water afforded relatively low catalytic activity and suffered difficulties in separation and recovery. A cation-exchange resin-supported Pt catalyst, with a high Pt loading of 15.6 wt-%, was applied for the continuous-flow oxidation of HMF to FDCA in water, affording high catalytic performance and long-term resistance [41].

Recently, water-soluble thermosensitive polymers, with a smart feature of reversible solubility changes upon temperature variation, have attracted extensive attention because of their great potential in targeted drug delivery [42,43], enzyme immobilization [44–46], and chemical catalysis [47–50]. By changing the system temperature, it is highly desirable to realize a reaction process of "quasi-homogeneous catalysis, heterogeneous recycle" using such smart polymer supported nanocatalysts. Consequently, herein we explored a novel thermoresponsive block copolymer containing imidazole groups, with an upper critical solution temperature (UCST) of about 45 °C, for use as a support to stabilize Pt nanoparticles. The produced Pt nanocatalysts were evaluated in the base-free oxidation of HMF toward FDCA by molecular oxygen in water. They were well water-dispersed and exhibited high catalytic activity above the UCST. And they could be easily recovered for reuse by decreasing the system temperature to below the UCST. This preliminary study may shed light on the development of base-free HMF catalytic oxidation systems as well as that of new thermoresponsive nanocatalysts.

2 Experimental

2.1 Materials

Acrylamide (99%) was obtained from Energy Chemical and recrystallized from acetone before use. Acrylonitrile (99%) was provided by Aladdin Chemicals Co., Ltd. and purified by 8 wt-% NaOH aqueous solution. 2,2-Azobisisobutyronitrile (AIBN, AR) was purchased from Wako Pure Chemical Ind., Ltd. and recrystallized from ethanol. *N*-Vinylimidazole (99%) was supplied by Macklin Biochemical Co., Ltd. in Shanghai. Hexachloroplatinic acid hexahydrate ($H_2PtCl_6 \cdot 6H_2O$, AR) was obtained from Aldrich. HMF (97%) and FDCA (98%) were supplied by Heowns Biochemical Technology Co., Ltd. 5-Hydroxymethyl-2-furancarboxylic acid (HMFCA, 98%) was obtained from Matrix Scientific. 5-Formyl-2-furancarboxylic acid (FFCA, 98%) was purchased from Toronto Research Chemicals Inc. 2,5-Diformylfuran (DFF, 98%) was provided by Sun Chemical Technology Co., Ltd.

2.2 Characterization

The fourier transform infrared spectroscopy (FTIR) spectra were collected on a Bruker Tensor 27 spectrometer. The ^1H nuclear magnetic resonance (NMR) spectrum was obtained with a Varian Mercury Vx-300 (300 MHz) spectrometer. The turbidity measurements were performed at 500 nm using an ultraviolet-visible (UV-Vis) spectrophotometer (Shimadzu UV-2550) equipped with a Shimadzu TCC-240A temperature controller and deionized water was used as a reference for 100% transmittance. The transmission electron microscopy (TEM) images of the specimens were obtained on an FEI Tecnai G2 F20 electron microscope with an accelerating voltage of 200 kV. The X-ray photoelectron spectroscopy (XPS) characterization of the Pt catalyst was performed on a Kratos Axis Ultra DLD spectrometer with a monochromatic Al Kα X-ray source ($h\nu$ = 1486.6 eV). The scanning electron microscopy (SEM) images of the specimens were obtained on a JEOL JSM-7500F field-emission scanning electron microscope. The contents of Pt in the catalysts as well as in the reaction solutions were determined by inductively coupled plasma-atomic emission spectrometry (ICP-AES) on an ICP-9000 (N + M) spectrometer (TJA Co.). The pH values were measured by means of a Rex PHS-3C pH meter with an E-201-C pH electrode. Conversions and product yields were determined by high-performance liquid chromatography (HPLC) using an Agilent 1200 series liquid chromatograph equipped with a UV-Vis detector operating at 271 nm. A Sepax Carbomix H-NP10:8% column was used with a column temperature of 65 °C and a H_3PO_4

aqueous solution (1 mmol·L^{-1}) was applied as the mobile phase at a flow rate of 0.6 mL·min^{-1}.

2.3 Catalyst preparation

2.3.1 Synthesis of the block copolymer

The block copolymer was synthesized through a reversible addition-fragmentation chain transfer (RAFT) polymerization by using cumyl dithiobenzoate (CDB) as the RAFT agent and AIBN as the initiator (Scheme 1). CDB was synthesized as described previously [41].

First, dithiobenzoate-terminated poly(acrylamide-*co*-acrylonitrile), denoted as **P1**, was synthesized as follows. In a 25-mL Schlenk flask, acrylamide (5 mmol) and acrylonitrile (3 mmol) were dissolved in dimethylsulfoxide (DMSO, 5 mL). Then AIBN (0.08 mmol) and CDB (0.04 mmol) were added, and the resulting reaction mixture was stirred for 0.5 h under N_2 atmosphere at room temperature, followed by being heated to 80 °C for 48 h. Thereafter, the mixture was cooled to room temperature. The produced polymer was precipitated in methanol, separated by filtration, and washed with methanol. After drying at 60 °C under vacuum, the yellowish solid **P1** was obtained. FTIR: 3430, 3345, 3197 (ν_{N-H}); 2930 (ν_{C-H}); 2242 ($\nu_{C\equiv N}$); 1667 ($\nu_{C=O}$) cm^{-1}.

Then, to a solution of **P1** (250 mg) in DMSO (5 mL) was added *N*-vinylimidazole (4 mmol) and AIBN (0.04 mmol). The reaction mixture was stirred for 0.5 h under N_2 atmosphere at room temperature and then heated to 80 °C for 48 h, followed by being cooled to room temperature. The block copolymer, poly(acrylamide-*co*-acrylonitrile)-*b*-poly(*N*-vinylimidazole), denoted as **P2**, was then obtained as a yellowish powder by precipitation with acetone, filtration, washing with acetone, and drying at 60 °C under vacuum. FTIR: ~3400, 3197 (ν_{N-H}); 3105 ($\nu_{=C-H}$); 2930 (ν_{C-H}); 2242 ($\nu_{C\equiv N}$); 1667 ($\nu_{C=O}$); 1497 ($\nu_{C=C}$) cm^{-1}. ^{1}H NMR (300 MHz, DMSO): δ (ppm) 1.4–2.2 (–CH_2–), 2.6–3.3 (–CH–), 6.5–7.5 (= C–H).

2.3.2 Synthesis of **P2**-stabilized Pt nanocatalysts

In a typical synthesis, an ethylene glycol solution of $H_2PtCl_6 \cdot 6H_2O$ (38 mmol·L^{-1}, 4.0 mL) and an aqueous solution of NaOH (2.5 mol·L^{-1}, 1.0 mL) were added in ethylene glycol (5 mL) with vigorous stirring for 0.5 h under N_2 atmosphere. The resulted orange-yellow solution was then heated to 160 °C and kept for 3 h, followed by being cooled to room temperature. The Pt nanoparticles were precipitated by adjusting the pH of the solution lower than 4.0 with a diluted HCl solution (1.0 mol·L^{-1}) and collected by centrifugation. After washing with deionized water thrice, the Pt nanoparticles were re-dispersed in deionized water (10 mL). Afterward, to an aqueous solution of a certain amount of **P2** (9 mL) was added the above-mentioned Pt dispersion (1 mL). The reaction mixture was stirred at 60 °C for 2 h. The product was precipitated by cooling the reaction mixture to room temperature, separated by centrifugation, washed thrice with deionized water, and then re-dispersed in deionized water (10 mL). The resulting specimen was denoted as Pt/**P2**-*x* (*x* = 20, 40, 60, 80) solution, where *x* represents the amount of **P2** used in the synthesis procedure (mg). The ICP-AES analysis determined that the Pt concentration in the sample was 1.5 mmol·L^{-1}. And the control experiment showed that there was no detectable Pt species in the aqueous solution after isolating Pt/**P2**-*x* from the sample.

For comparison, Pt/**P1** was also synthesized according to the above-mentioned procedure by the replacement of **P2** by **P1** (40 mg).

2.4 HMF oxidation

A typical procedure for HMF oxidation reaction was as

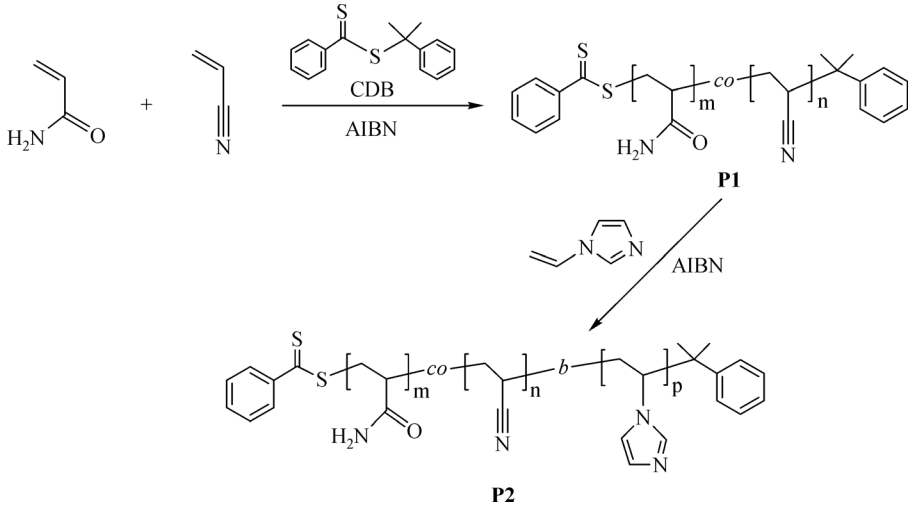

Scheme 1 Synthesis of the block copolymer **P2**.

follows. A solution of HMF (0.075 mmol) in deionized water (3 mL) and the above-synthesized Pt/**P2**-*x* solution (2 mL) were charged into a 30-mL stainless steel autoclave equipped with a magnetic stirring bar. After being purged with pure O_2 for five times, the autoclave was pressurized to the desired pressure with O_2 (2–8 bar) and immersed into a pre-heated oil bath with the reaction mixture being stirred. After the reaction was over, the catalyst was precipitated by cooling the reaction mixture to room temperature, separated by centrifugation, and washed with deionized water. The liquid phase was subjected to HPLC analysis. For the recycling experiment, the recovered Pt nanocatalyst was re-dissolved in deionized water and subjected to a new run with fresh reactants under the same reaction conditions.

3 Results and discussion

3.1 Catalyst characterization

The as-synthesized Pt/**P2**-*x* catalysts were characterized by TEM. Figure 1 shows the typical TEM image of Pt/**P2**-40. Uniformly dispersed Pt nanoparticles were observed. The histogram of particle size distribution, based on the measurement of more than 150 Pt nanoparticles, indicated a very narrow size distribution of Pt nanoparticles in the range of 1.3–2.4 nm with an average particle size of ca. 1.9 nm. Similar TEM results were obtained for other catalysts.

The Pt 4f XPS spectrum of Pt/**P2**-40 is depicted in Fig. 2. Two peaks ascribed to Pt $4f_{7/2}$ and Pt $4f_{5/2}$ were observed, which could be deconvoluted into four sub-bands. The components located at about 70.7 and 74.1 eV could be assigned to Pt $4f_{7/2}$ and Pt $4f_{5/2}$ of Pt^0, respectively. And the minor components appeared at about 71.8 and 75.4 eV could be attributed to Pt^{2+} species. The results of XPS characterization indicated that Pt predominantly existed as Pt^0 species in the catalyst, along with about 30% of oxidized Pt^{2+} species.

The thermoresponsive properties of the catalysts Pt/**P2**-*x* were investigated by the measurement of the turbidity in 0.5 wt-% aqueous solutions with the observation of the 500 nm UV transmittance. Figure 3 shows the representative turbidity curves for the 0.5 wt-% aqueous solutions of **P2** and Pt/**P2**-40. Both the two specimens showed a UCST of about 45 °C and a rapid decrease in the transmittance of the solutions was observed as lowering the temperature from 50 °C to 40 °C. For the purpose of comparison, the thermoresponsive property of polymer **P1** was also tested. As shown in Fig. S1 (cf. Electronic Supplementary Material, ESM), **P1** exhibited an almost identical turbidity curve to **P2**, suggesting that the thermosensitivity was mainly contributed by the segment of poly(acrylamide-*co*-acrylonitrile). The observed phase transition behavior was associated with the enhanced inter-/intra-chain hydrogen bonding interaction between the carbonyl and amino groups upon cooling [51], which forced the polymer to appear in a collapsed globule structure and precipitated from water. As a consequence, Pt/**P2**-40 was well-dispersed in deionized water at 55 °C but precipitated at 35 °C. This thermoresponsive character is highly desirable for HMF oxidation reaction that is often performed at a temperature higher than this UCST.

3.2 Reaction pathways for base-free oxidation of HMF to FDCA over Pt/**P2**-*x*

The as-synthesized catalysts Pt/**P2**-*x* were evaluated in the aqueous-phase aerobic oxidation of HMF to FDCA without the assistance of any base additive. For the purpose of comparison, polymer **P2** was also investigated under the identical reaction conditions. No HMF conversion was detected (Table 1, entry 1), indicating that the polymer was catalytically inactive in this reaction system.

Figure 4 shows the reaction profiles for HMF oxidation over Pt/**P2**-40 at 100 °C under O_2 pressure of 8 bar. FFCA and DFF were the major intermediate products for this reaction system, along with a very little amount of

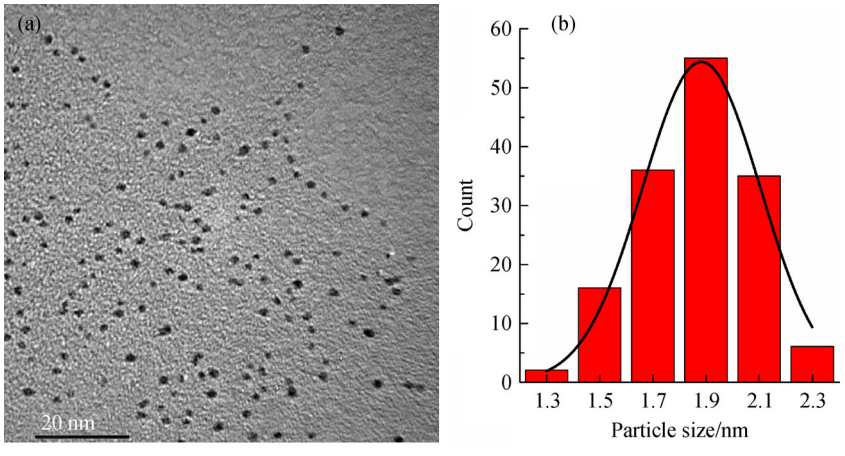

Fig. 1 (a) TEM image and (b) particle size distribution of Pt/**P2**-40.

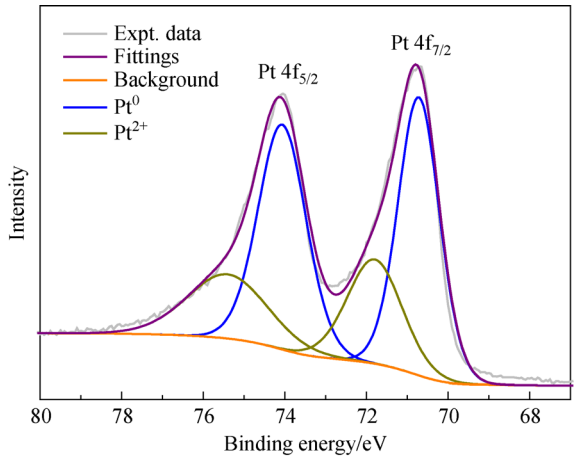

Fig. 2 Pt 4f XPS spectrum of Pt/**P2**-40.

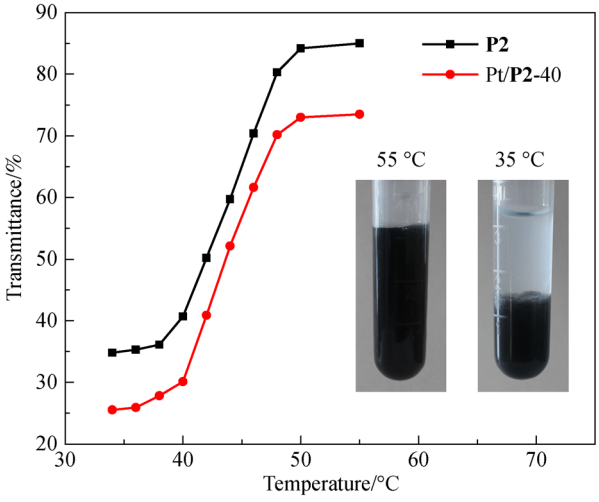

Fig. 3 The temperature-dependence of the turbidity for the 0.5 wt-% aqueous solution of **P2** and Pt/**P2**-40. The insets are the photographs of Pt/**P2**-40 aqueous solution at 55 °C and 35 °C.

HMFCA (< 1%) detected within the first 1 h. The yield of DFF reached 15% in 1 h and began to decrease to zero after 6 h of reaction. And the yield of FFCA reached 54% within 2 h and then underwent a continuous decline. A complete conversion of HMF was achieved in 6 h, and the yield of FDCA monotonically increased with prolonging the reaction time, reaching > 99.9% after 12 h. All these observations suggested that the formation of DFF intermediate via oxidation of the hydroxymethyl group in HMF was the dominant pathway for HMF oxidation over Pt/**P2**-*x* catalysts (Scheme 2).

It was reported that the soluble base had a dramatic impact on the aldehyde oxidation by the formation of a geminal diol intermediate and its consequent dehydrogenation conversion toward a carboxylic acid function, thus HMFCA was always generated as one of the major intermediate products in the presence of a liquid base [13–23,52]. While the present reaction solution showed a rather moderate pH of 7.5 in the initial period, which sharply decreased to about 3.0 after 2 h of reaction due to the production of the acidic products, including FFCA and FDCA. On the other hand, Pt nanocatalysts had been reported to be highly effective for the aerobic oxidation of the alcohol function in HMF by promoting the activation of the C–H bond in the hydroxymethyl group and facilitating the elimination of *β*-H atom to form an aldehyde group [17,31,40]. Therefore, DFF was formed initially as a reaction intermediate for Pt/**P2**-*x* catalyzed base-free aerobic oxidation of HMF.

Based on the reaction results, it could be concluded that HMF was rapidly oxidized by Pt/**P2**-*x* to produce DFF, followed by a continuous oxidation to generate FFCA and further FDCA. The relatively low yield of DFF throughout the reaction indicated that the oxidation process of DFF to FFCA was fast. Whereas on the contrary, FFCA was the main product during the initial reaction stage with a higher yield than DFF and FDCA, suggesting that the conversion of FFCA to FDCA was the slowest step in the entire oxidation process from HMF to FDCA.

Table 1 Catalytic performance of different catalyst systems for the aerobic oxidation of HMF [a)]

Entry	Catalyst	PI/μmol [b)]	HMF conv./%	Yield/%			
				HMFCA	DFF	FFCA	FDCA
1	**P2**	0	0	0	0	0	0
2	Pt/**P2**-40	0	100	0	0	0	> 99.9
3	Pt/**P1**	0	79.4	0	12.5	20.2	46.7
4	Pt/**P1**	5	63.4	4.5	2.8	40.3	15.8
5	Pt/**P1**	50	55.9	3.3	5.0	34.6	13.1
6	Pt/**P1**	300	40.6	2.0	2.9	25.4	10.2
7	Pt/**P2**-20	0	100	0	0	11.8	88.2
8	Pt/**P2**-60	0	100	0	0	10.9	89.1
9	Pt/**P2**-80	0	100	0	4.6	41.6	53.8

a) Reaction conditions: HMF/Pt molar ratio = 25, O_2 8 bar, 100 °C, 12 h; (b) PI: 1-propylimidazole.

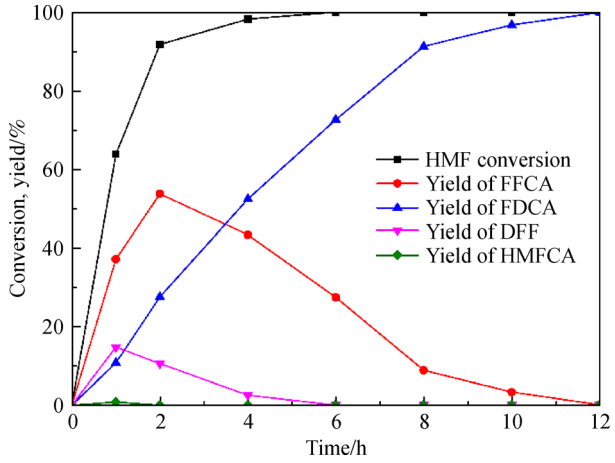

Fig. 4 Evolution of the concentrations of HMF and the products as a function of reaction time over Pt/**P2**-40 (reaction conditions: HMF/Pt molar ratio = 25, O_2 8 bar, 100 °C).

3.3 The role of imidazole functional group in **P2** on aerobic oxidation of HMF

To investigate the role of the imidazole functional groups in polymer **P2**, a control experiment with Pt/**P1** as the catalyst was performed. As shown in Table 1, Pt/**P1** exhibited notably inferior catalytic performance compared with Pt/**P2**-40, giving a low FDCA yield of 46.7% with an HMF conversion of 79.4% after 12 h (Table 1, entry 3). This indicated that the presence of imidazole groups in the polymer could significantly enhance the catalytic behavior of the catalyst.

For a further comparison, a certain amount of PI, a weak organic base with a similar structure to the imidazole groups in polymer **P2**, was added into the reaction system catalyzed by Pt/**P1**. Interestingly, it was found that the addition of PI did not facilitate the catalytic reaction; conversely, it had a distinct inhibiting effect on the catalytic activity of Pt nanocatalyst. The presence of even a small amount (5 μmol) of PI caused a significant decrease in FDCA yield (Table 1, entry 4). In addition, this inhibiting effect became stronger with the increase in the amount of PI. When 50 μmol of PI, which was approximately equivalent to the amount of imidazole groups in the catalyst of Pt/**P2**-40, was added, the yield of FDCA decreased further to 13.1% (Table 1, entry 5). Furthermore, a certain amount of HMFCA arose in the products when PI was used. This inhibiting effect may be derived from the competitive adsorption of PI molecules and reactants on the surface of Pt nanoparticles, which led to lower probability of contact between reactants and catalytic active sites, thus resulting in inferior catalytic efficiency.

Based on these comparison results, we could then conclude that combining the imidazole groups into the polymer structure produced a promising carrier of Pt for the liquid-base-free oxidation of HMF. The promotion of catalytic activity by the imidazole groups in polymer **P2** was probably associated with the π–π interaction between the imidazole ring and furan ring, leading to the enrichment of reactants surrounding the polymer molecules.

It is noteworthy that the RAFT polymerization with CDB represents a living radical polymerization process, which allows the facile synthesis of block copolymers and makes it possible to design target polymers at the molecular level. The segment of poly(acrylamide-*co*-acrylonitrile) derived from the copolymerization of acrylamide and acrylonitrile was responsible for the distinct thermosensitivity of polymer **P2**, where the UCST could be regulated by tuning the molar ratio of acrylamide to acrylonitrile. Whereas the segment of poly(*N*-vinylimidazole) was beneficial for promotion of the catalytic activity of Pt/**P2**-*x*. By using this strategy, it is highly promising to design diverse thermoresponsive polymers as catalysts or catalyst supports for varying catalytic processes.

3.4 Effect of the ratio of **P2** to Pt on catalytic performance

To study the influence of the ratio of **P2** to Pt in the catalyst on the catalytic performance, the supported catalysts Pt/**P2**-*x* with different amounts of polymer **P2** were evaluated in the oxidation of HMF. Pt/**P2**-40 exhibited the best catalytic performance, giving a high FDCA yield of > 99.9% after 12 h (Table 1, entry 2). With further increasing the ratio of polymer to Pt, a gradual decline in catalytic activity was observed (Table 1, entries 8 and 9). For example, the yield of FDCA decreased to 53.8% over Pt/**P2**-80 under the same reaction conditions, along with 4.6% unconverted DFF. The decrease in catalytic perfor-

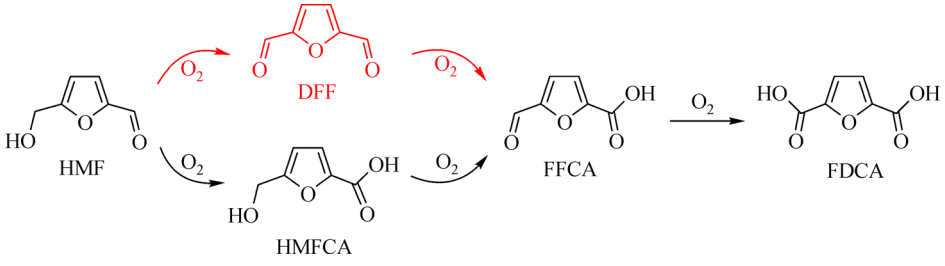

Scheme 2 Reaction pathways for the aerobic oxidation of HMF to FDCA over Pt/**P2**-*x*.

mance may be related to the enhanced steric hindrance for reactant access to the surface of Pt nanoparticles that were surrounded by more polymer segments. When the catalyst of Pt/**P2**-20, with a relatively low ratio of **P2** to Pt, was used, lower reaction activity compared with Pt/**P2**-40 was also presented (Table 1, entry 7). The TEM characterization showed that Pt nanoparticles were well dispersed without agglomeration with an average particle size of ca. 2.0 nm for the catalyst Pt/**P2**-20 after being used in the oxidation reaction of HMF (Fig. S2, cf. ESM), suggesting that this amount of polymer was able to effectively stabilize Pt nanoparticles. Thus the inferior catalytic activity of Pt/**P2**-20 may be associated with the relatively low content of imidazole groups in Pt/**P2**-20.

3.5 Effects of O_2 pressure and reaction temperature on catalytic performance

The effects of O_2 pressure and reaction temperature on the catalytic performance were investigated by using Pt/**P2**-40 as a model catalyst. HMF achieved a complete conversion in 12 h for all the cases studied. However, as shown in Fig. 5, obvious dependences of the FDCA yield on the O_2 pressure and reaction temperature were observed. When the O_2 pressure was raised from 2 to 8 bar, an increase in the yield of FDCA from 80.1% to > 99.9% was achieved (Fig. 5(a)). Oxygen was believed to serve as a sacrificial electron acceptor and consume excess electrons on the Pt surface generated from the three-step oxidant reaction from HMF to FDCA [52,53]. The present results indicated that within the studied O_2 pressure range, more O_2 in the reaction system could facilitate the reaction. By increasing the reaction temperature from 70 °C to 100 °C, the yield of FDCA increased from 63.4% to > 99.9% (Fig. 5(b)). It should be noted that the catalytic performance achieved over the present catalyst Pt/**P2**-40 is at the high level as compared with those of diverse noble metal nanocatalysts previously reported for the base-free oxidation of HMF in neat water under O_2 atmosphere (Table S1, cf. ESM).

3.6 Catalyst recycling and stability

The stability and reusability of Pt/**P2**-*x* catalysts in the aerobic oxidation of HMF were investigated using Pt/**P2**-40 as a model catalyst (Fig. 6). As described above, the catalyst Pt/**P2**-40 possessed a thermoresponsive phase transition behavior in aqueous solution with a UCST of about 45 °C. That is, it was well dispersed during the oxidation reaction carried out at 100 °C (Fig. 6(a)). After the oxidation reaction, it could be precipitated from the reaction mixture by cooling the reaction system to room temperature and recovered for reuse (Fig. 6(b)).

As shown in Fig. 6(c), the catalyst still remained high catalytic performance after five cycles with an FDCA yield of 95.7%, though a gradual and slight decrease in the yield of FDCA occurred during the durability test. The ICP-AES analysis showed that the Pt content in the supernatant after each cycle was less than 1.2 $mg \cdot L^{-1}$, corresponding to a Pt leaching of no more than 1%. This indicated that the catalyst Pt/**P2**-40 could be well recovered from the reaction mixture based on its thermosensitivity. Characterization of the used catalyst by TEM disclosed that Pt nanoparticles were still homogeneously dispersed with no obvious agglomeration and their average particle size remained relatively constant at about 2.0 nm (Fig. 7), suggesting the high stability of the present Pt catalyst in the aerobic

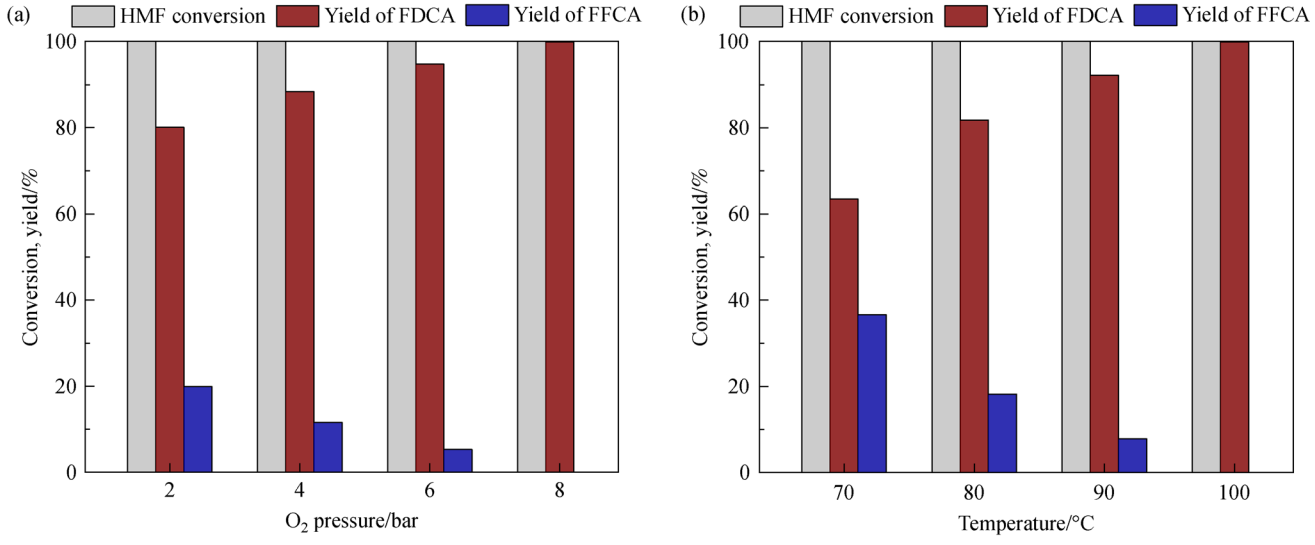

Fig. 5 (a) Influence of O_2 pressure on the base-free aerobic oxidation of HMF (reaction conditions: HMF/Pt molar ratio = 25, 12 h, 100 °C); (b) influence of reaction temperature on the base-free aerobic oxidation of HMF (reaction conditions: HMF/Pt molar ratio = 25, 12 h, O_2 8 bar).

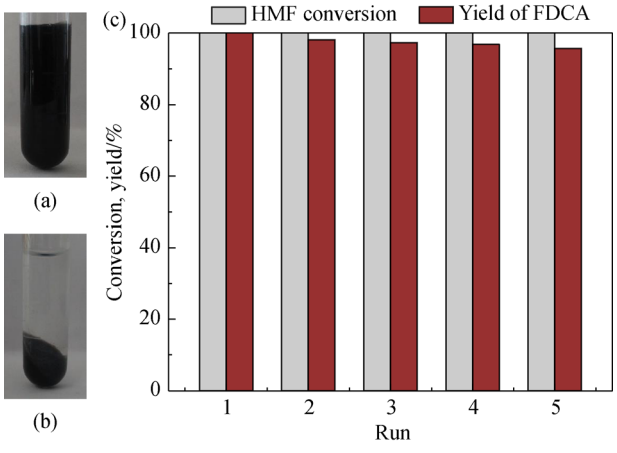

Fig. 6 Photographs of the reaction mixture (a) under the reaction temperature and (b) after cooling to room temperature; (c) recycling tests of Pt/**P2**-40 for the base-free aerobic oxidation of HMF.

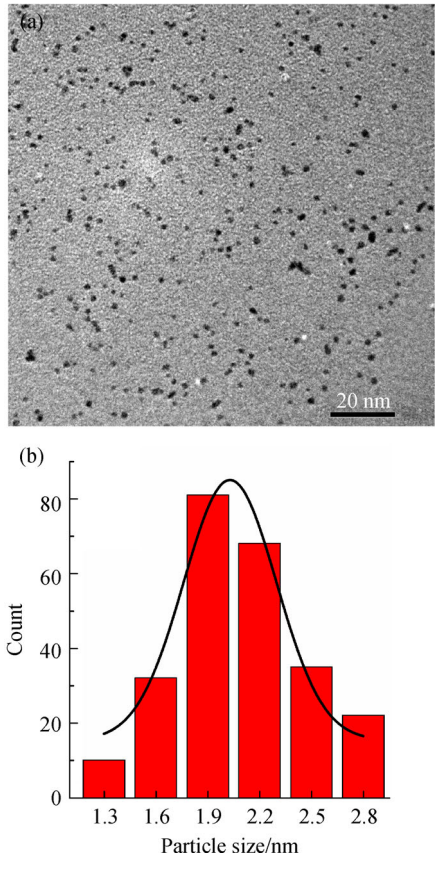

Fig. 7 (a) TEM image and (b) particle size distribution of used Pt/**P2**-40 catalyst.

oxidation system. The results of SEM and FTIR analyses, as shown in Figs. S3 and S4 (cf. ESM) respectively, also demonstrated that the catalyst showed no obvious change after undergoing the oxidation reaction.

4 Conclusions

The imidazole-containing thermoresponsive block copolymer **P2** with a UCST of about 45 °C was synthesized through RAFT polymerization and applied to stabilize Pt nanoparticles, affording a kind of effective Pt nanocatalysts for the liquid-base-free aerobic oxidation of HMF toward FDCA in water. The supported Pt nanocatalysts Pt/**P2**-*x*, with a similar UCST to the block copolymer, were well-dispersed and formed a quasi-homogeneous catalytic system for the oxidation reaction, providing high catalytic performance. Especially, the catalyst Pt/**P2**-40 exhibited the best catalytic activity with FDCA yields up to > 99.9%. The oxidation reaction proceeded via DFF and FFCA formation to produce FDCA and the promotion of catalytic activity by the imidazole functional groups in **P2** was determined. Moreover, a heterogeneous separation and recovery of catalyst could be easily realized after the reaction by cooling down the reaction mixture below the UCST. The Pt catalysts showed good stability and reusability, and could be reused for five times with a slight loss in catalytic activity. These results suggested a great potential for industrial application of these thermoresponsive block copolymer supported nanocatalysts. More importantly, it is facile to alter the property of the block copolymer, by adjusting the composition of polymer chain segments, to widen its applications in other catalytic systems.

Acknowledgements This work was financially supported by the National Natural Science Foundation of China (Grant No. 21203102), the Nankai University & Cangzhou Bohai New Area Institute of Green Chemical Engineering Fund (Grant No. NCC2020PY02), the Tianjin Municipal Natural Science Foundation (Grant No. 17JCYBJC22600), the Innovative Team Project of Ministry of Education of China (IRT13R30), and the Fundamental Research Funds for the Central Universities.

Electronic Supplementary Material Supplementary material is available in the online version of this article at https://dx.doi.org/10.1007/s11705-021-2092-4 and is accessible for authorized users.

References

1. Besson M, Gallezot P, Pinel C. Conversion of biomass into chemicals over metal catalysts. Chemical Reviews, 2014, 114(3): 1827–1870
2. Li C, Zhao X, Wang A, Huber G W, Zhang T. Catalytic transformation of lignin for the production of chemicals and fuels. Chemical Reviews, 2015, 115(21): 11559–11624
3. Liu B, Zhang Z. Catalytic conversion of biomass into chemicals and fuels over magnetic catalysts. ACS Catalysis, 2016, 6(1): 326–338
4. Zhang Z, Song J, Han B. Catalytic transformation of lignocellulose into chemicals and fuel products in ionic liquids. Chemical Reviews, 2017, 117(10): 6834–6880
5. Zhang Z, Huber G W. Catalytic oxidation of carbohydrates into organic acids and furan chemicals. Chemical Society Reviews,

2018, 47(4): 1351–1390
6. van Putten R J, van der Waal J C, de Jong E, Rasrendra C B, Heeres H J, de Vries J G. Hydroxymethylfurfural, a versatile platform chemical made from renewable resources. Chemical Reviews, 2013, 113(3): 1499–1597
7. Xu C, Paone E, Rodríguez-Padrón D, Luque R, Mauriello F. Recent catalytic routes for the preparation and the upgrading of biomass derived furfural and 5-hydroxymethylfurfural. Chemical Society Reviews, 2020, 49(13): 4273–4306
8. Tong X, Ma Y, Li Y. Biomass into chemicals: conversion of sugars to furan derivatives by catalytic processes. Applied Catalysis A, General, 2010, 385(1–2): 1–13
9. Werpy T, Petersen G. Top Value Added Chemicals from Biomass: Volume I—Results of Screening for Potential Candidates from Sugars and Synthesis Gas. US DOE Report, 2004
10. Eerhart A J J E, Faaij A P C, Patel M K. Replacing fossil based PET with biobased PEF; process analysis, energy and GHG balance. Energy & Environmental Science, 2012, 5(4): 6407–6422
11. Sajid M, Zhao X, Liu D. Production of 2,5-furandicarboxylic acid (FDCA) from 5-hydroxymethylfurfural (HMF): recent progress focusing on the chemical-catalytic routes. Green Chemistry, 2018, 20(24): 5427–5453
12. Chen C, Wang L, Zhu B, Zhou Z, El-Hout S I, Yang J, Zhang J. 2,5-Furandicarboxylic acid production via catalytic oxidation of 5-hydroxymethylfurfural: catalysts, processes and reaction mechanism. Journal of Energy Chemistry, 2021, 54: 528–554
13. Albonetti S, Lolli A, Morandi V, Migliori A, Lucarelli C, Cavani F. Conversion of 5-hydroxymethylfurfural to 2,5-furandicarboxylica-cid over Au-based catalysts: optimization of active phase and metal-support interaction. Applied Catalysis B: Environmental, 2015, 163: 520–530
14. Cai J, Ma H, Zhang J, Song Q, Du Z, Huang Y, Xu J. Gold nanoclusters confined in a supercage of Y zeolite for aerobic oxidation of HMF under mild conditions. Chemistry-A European Journal, 2013, 19(42): 14215–14223
15. Liu Y, Ma H Y, Lei D, Lou L L, Liu S, Zhou W, Wang G C, Yu K. Active oxygen species promoted catalytic oxidation of 5-hydroxymethyl-2-furfural on facet-specific Pt nanocrystals. ACS Catalysis, 2019, 9(9): 8306–8315
16. Yu K, Lei D, Feng Y, Yu H, Chang Y, Wang Y, Liu Y, Wang G C, Lou L L, Liu S, Zhou W. The role of Bi-doping in promoting electron transfer and catalytic performance of Pt/3DOM-$Ce_{1-x}Bi_xO_{2-\delta}$. Journal of Catalysis, 2018, 365: 292–302
17. Rass H A, Essayem N, Besson M. Selective aerobic oxidation of 5-HMF into 2,5-furandicarboxylic acid with Pt catalysts supported on TiO_2- and ZrO_2-based supports. ChemSusChem, 2015, 8(7): 1206–1217
18. Yang J, Yu H, Wang Y, Qi F, Liu H, Lou L L, Yu K, Zhou W, Liu S. Effect of the oxygen coordination environment of Ca-Mn oxides on the catalytic performance of Pd supported catalysts for aerobic oxidation of 5-hydroxymethyl-2-furfural. Catalysis Science & Technology, 2019, 9(23): 6659–6668
19. Lei D, Yu K, Li M R, Wang Y, Wang Q, Liu T, Liu P, Lou L L, Wang G, Liu S. Facet effect of single-crystalline Pd nanocrystals for aerobic oxidation of 5-hydroxymethyl-2-furfural. ACS Catalysis, 2017, 7(1): 421–432
20. Zhang Z, Zhen J, Liu B, Lv K, Deng K. Selective aerobic oxidation of the biomass-derived precursor 5-hydroxymethylfurfural to 2,5-furandicarboxylic acid under mild conditions over a magnetic palladium nanocatalyst. Green Chemistry, 2015, 17(2): 1308–1317
21. Xie J, Nie J, Liu H. Aqueous-phase selective aerobic oxidation of 5-hydroxymethylfurfural on Ru/C in the presence of base. Chinese Journal of Catalysis, 2014, 35(6): 937–944
22. Villa A, Schiavoni M, Campisi S, Veith G M, Prati L. Pd-modified Au on carbon as an effective and durable catalyst for the direct oxidation of HMF to 2,5-furandicarboxylic acid. ChemSusChem, 2013, 6(4): 609–612
23. Gui Z, Cao W, Saravanamurugan S, Riisager A, Chen L, Qi Z. Efficient aerobic oxidation of 5-hydroxymethylfurfural in aqueous media with Au-Pd supported on zinc hydroxycarbonate. ChemCatChem, 2016, 8(23): 3636–3643
24. Gupta N K, Nishimura S, Takagaki A, Ebitani K. Hydrotalcite-supported gold-nanoparticle-catalyzed highly efficient base-free aqueous oxidation of 5-hydroxymethylfurfural into 2,5-furandicarboxylic acid under atmospheric oxygen pressure. Green Chemistry, 2011, 13(4): 824–827
25. Gao T, Gao T, Fang W, Cao Q. Base-free aerobic oxidation of 5-hydroxymethylfurfural to 2,5-furandicarboxylic acid in water by hydrotalcite-activated carbon composite supported gold catalyst. Molecular Catalysis, 2017, 439: 171–179
26. Ferraz C P, Zieliński M, Pietrowski M, Heyte S, Dumeignil F, Rossi L M, Wojcieszak R. Influence of support basic sites in green oxidation of biobased substrates using Au-promoted catalysts. ACS Sustainable Chemistry & Engineering, 2018, 6(12): 16332–16340
27. Wang Y, Yu K, Lei D, Si W, Feng Y, Lou L L, Liu S. Basicity-tuned hydrotalcite-supported Pd catalysts for aerobic oxidation of 5-hydroxymethyl-2-furfural under mild conditions. ACS Sustainable Chemistry & Engineering, 2016, 4(9): 4752–4761
28. Gao Z, Xie R, Fan G, Yang L, Li F. Highly efficient and stable bimetallic AuPd over La-doped Ca-Mg-Al layered double hydroxide for base-free aerobic oxidation of 5-hydroxymethylfurfural in water. ACS Sustainable Chemistry & Engineering, 2017, 5(7): 5852–5861
29. Bonincontro D, Lolli A, Villa A, Prati L, Dimitratos N, Veith G M, Chinchilla L E, Botton G A, Cavani F, Albonetti S. AuPd-nNiO as an effective catalyst for the base-free oxidation of HMF under mild reaction conditions. Green Chemistry, 2019, 21(15): 4090–4099
30. Wan X, Zhou C, Chen J, Deng W, Zhang Q, Yang Y, Wang Y. Base-free aerobic oxidation of 5-hydroxymethyl-furfural to 2,5-furandicarboxylic acid in water catalyzed by functionalized carbon nanotube-supported Au-Pd alloy nanoparticles. ACS Catalysis, 2014, 4(7): 2175–2185
31. Zhou C, Deng W, Wan X, Zhang Q, Yang Y, Wang Y. Functionalized carbon nanotubes for biomass conversion: the base-free aerobic oxidation of 5-hydroxymethylfurfural to 2,5-furandicarboxylic acid over platinum supported on a carbon nanotube catalyst. ChemCatChem, 2015, 7(18): 2853–2863
32. Yi G, Teong S P, Zhang Y. Base-free conversion of 5-hydroxymethylfurfural to 2,5-furandicarboxylic acid over a Ru/C catalyst. Green Chemistry, 2016, 18(4): 979–983
33. Guan W, Zhang Y, Wei Y, Li B, Feng Y, Yan C, Huo P, Yan Y.

Pickering HIPEs derived hierarchical porous nitrogen-doped carbon supported bimetallic AuPd catalyst for base-free aerobic oxidation of HMF to FDCA in water. Fuel, 2020, 278: 118362

34. Han X, Li C, Guo Y, Liu X, Zhang Y, Wang Y. N-doped carbon supported Pt catalyst for base-free oxidation of 5-hydroxymethylfurfural to 2,5-furandicarboxylic acid. Applied Catalysis A, General, 2016, 526: 1–8
35. Artz J, Palkovits R. Base-free aqueous-phase oxidation of 5-hydroxymethylfurfural over ruthenium catalysts supported on covalent triazine frameworks. ChemSusChem, 2015, 8(22): 3832–3838
36. Gao T, Chen J, Fang W, Cao Q, Su W, Dumeignil F. Ru/$Mn_xCe_1O_y$ catalysts with enhanced oxygen mobility and strong metal-support interaction: exceptional performances in 5-hydroxymethylfurfural base-free aerobic oxidation. Journal of Catalysis, 2018, 368: 53–68
37. Mishra D K, Lee H J, Kim J, Lee H S, Cho J K, Suh Y W, Yi Y, Kim Y J. $MnCo_2O_4$ spinel supported ruthenium catalyst for air-oxidation of HMF to FDCA under aqueous phase and base-free conditions. Green Chemistry, 2017, 19(7): 1619–1623
38. Han X, Geng L, Guo Y, Jia R, Liu X, Zhang Y, Wang Y. Base-free aerobic oxidation of 5-hydroxymethylfurfural to 2,5-furandicarboxylic acid over a Pt/C–O–Mg catalyst. Green Chemistry, 2016, 18 (6): 1597–1604
39. Ke C, Li M, Fan G, Yang L, Li F. Pt nanoparticles supported on nitrogen-doped-carbon-decorated CeO_2 for base-free aerobic oxidation of 5-hydroxymethylfurfural. Chemistry, an Asian Journal, 2018, 13(18): 2714–2722
40. Siankevich S, Savoglidis G, Fei Z, Laurenczy G, Alexander D T L, Yan N, Dyson P J. A novel platinum nanocatalyst for the oxidation of 5-hydroxymethylfurfural into 2,5-furandicarboxylic acid under mild conditions. Journal of Catalysis, 2014, 315: 67–74
41. Liguori F, Barbaro P, Calisi N. Continuous-flow oxidation of HMF to FDCA by resin-supported platinum catalysts in neat water. ChemSusChem, 2019, 12(12): 2558–2563
42. Bawa P, Pillay V, Choonara Y E, du Toit L C. Stimuli-responsive polymers and their applications in drug delivery. Biomedical Materials, 2009, 4(2): 022001
43. Cheng W, Gu L, Ren W, Liu Y. Stimuli-responsive polymers for anti-cancer drug delivery. Materials Science and Engineering C, 2015, 45: 600–608
44. Trzebicka B, Szweda R, Kosowski D, Szweda D, Otulakowski Ł, Haladjova E, Dworak A. Thermoresponsive polymer-peptide/protein conjugates. Progress in Polymer Science, 2017, 68: 35–76
45. Mackenzie K J, Francis M B. Recyclable thermoresponsive polymer-cellulase bioconjugates for biomass depolymerization. Journal of the American Chemical Society, 2013, 135(1): 293–300
46. Lou L L, Qu H, Yu W, Wang B, Ouyang L, Liu S, Zhou W. Covalently immobilized lipase on a thermoresponsive polymer with an upper critical solution temperature as an efficient and recyclable asymmetric catalyst in aqueous media. ChemCatChem, 2018, 10(5): 1166–1172
47. Zhang J, Zhang M, Tang K, Verpoort F, Sun T. Polymer-based stimuli-responsive recyclable catalytic systems for organic synthesis. Small, 2014, 10(1): 32–46
48. Tan R, Dong Y, Peng M, Zheng W, Yin D. Thermoresponsive chiral salen Mn(III) complexes as efficient and reusable catalysts for the oxidative kinetic resolution of secondary alcohols in water. Applied Catalysis A, General, 2013, 458: 1–10
49. Yu W, Lou L L, Yu K, Li S, Shi Y, Liu S. Pt nanoparticles stabilized by thermosensitive polymer as effective and recyclable catalysts for asymmetric hydrogenation of ethyl pyruvate. RSC Advances, 2016, 6(57): 52500–52508
50. Kong L, Zhao J, Cheng T, Lin J, Liu G. A polymer-coated rhodium/diamine-functionalized silica for controllable reaction switching in enantioselective tandem reduction-actonization of ethyl 2-acylarylcarboxylates. ACS Catalysis, 2016, 6(4): 2244–2249
51. Hou L, Wu P. Understanding the UCST-type transition of P(AAm-co-AN) in H_2O and D_2O: dramatic effects of solvent isotopes. Soft Matter, 2015, 11(35): 7059–7065
52. Davis S E, Zope B N, Davis R J. On the mechanism of selective oxidation of 5-hydroxymethylfurfural to 2,5-furandicarboxylic acid over supported Pt and Au catalysts. Green Chemistry, 2012, 14(1): 143–147
53. Davis S E, Ide M S, Davis R J. Selective oxidation of alcohols and aldehydes over supported metal nanoparticles. Green Chemistry, 2013, 15(1): 17–45